Applied Physics Express

LETTER

High-efficiency generation of a low-noise laser at 447 nm

Applied Physics Express 12, 032010 (2019)
https://doi.org/10.7567/1882-0786/aafed8

LETTER

High-efficiency generation of a low-noise laser at 447 nm

Xiaojie Zuo[1], Zhihui Yan[1,2*], and Xiaojun Jia[1,2]

[1]State Key Laboratory of Quantum Optics and Quantum Optics Devices, Institute of Opto-Electronics, Shanxi University, Taiyuan, 030006, People's Republic of China
[2]Collaborative Innovation Center of Extreme Optics, Shanxi University, Taiyuan 030006, People's Republic of China

*E-mail: zhyan@sxu.edu.cn

Received November 15, 2018; accepted January 13, 2019; published online February 25, 2019

We experimentally present a high-efficiency generation of low-noise 447 nm laser by frequency doubling of a Ti:sapphire laser in an external ring cavity with a PPKTP crystal. The maximum blue laser power of 308 mW has been obtained and the corresponding conversion efficiency can reach 70%, when 440 mW infrared laser is injected. Moreover, the noise of the resulting blue laser can reach the quantum noise limit when the analyzing frequency is above 1.5 MHz. Our system provides an ideal pump field for an optical parametric amplifier for the generation of non-classical states of light matching matter absorption line. © 2019 The Japan Society of Applied Physics

The non-classical state of light is the building block of quantum metrology and quantum information science.[1–3] In quantum metrology, the squeezed state of light can improve the sensitivity of magnetic field measurements in atom systems.[4] In the quantum internet, consisting of quantum nodes and quantum channels, quantum nodes can process and store quantum information;[5] meanwhile, quantum channels enable the transfer of quantum information and connect quantum nodes.[6–8] In particular, multipartite entangled optical modes enable to entangle multiple distant quantum nodes for the application of quantum network protocols,[9,10] and can be prepared by means of coupling multiple squeezed optical beams on a beam splitter network.[11] Thus, research regarding the generation of squeezed states of light resonant with atomic absorption lines are widely carried out for quantum metrology and quantum interface between quantum nodes and quantum channels. An optical parametric amplifier (OPA) is an effective device to produce a squeezed state of light,[12,13] while the laser with the shorter visible wavelength is required to pump the OPA. Therefore, the high-efficiency generation of a continuous-wave single-frequency blue laser with low noise is essential for preparing squeezed light resonant with an atomic absorption line; in addition to its industrial applications of laser printing and lithography, this can be applied in scientific research, such as quantum metrology[14,15] and quantum information.[16,17]

A laser with a shorter visible wavelength can be produced by frequency doubling of an infrared laser based on the second harmonic generation (SHG) process.[18,19] A periodically poled potassium titanyle phosphate (PPKTP) crystal with its advantages of the high effective nonlinearity and no walk-off is one of the well-established nonlinear crystals.[20] The external cavity frequency doubling can enhance the nonlinear interaction for producing blue laser.[21,22] At present, rubidium (Rb) and cesium (Cs) atoms are well understood atomic media for quantum metrology and quantum information.[23–27] Thus, the production of 398 nm laser has been experimentally realized,[28] which is used as the pump field of OPA for the generation of non-classical state of light resonant with Rb atoms. The thermal effects, including the thermal lensing effect and thermal induced bistability, occur in the SHG progress. The thermal lensing effect associated with the SHG process limits the conversion efficiency. The SHG laser propagates in the crystal over and over, and leads a severe thermal loading. Both the volumetric heating and surface temperature controlling lead to a temperature gradient, and form a thermal lens in the nonlinear crystal. The thermal lensing effect will deform the spatial mode of the SHG cavity and influence the mode matching of the fundamental wave to the SHG cavity. Therefore, the overall SHG conversion efficiency will be decreased if the thermal lensing effect deteriorates the mode matching condition. The thermal loading of the crystal also causes optical bistability, which makes the locking of the SHG cavity at the top of the peaks hard. The heating will form a thermal gradient inside the crystal and result in asymmetry of the resonant signal, therefore the deterioration of the error signal will make it challenging for the SHG cavity to be actively locked to its fringe maximum at high powers. The wavelength of 398 nm is at the transmission cut-off wavelength of the PPKTP crystal and the thermal effect is severe. For the generation of the 398 nm laser, the severe thermal and grey tracking effects limit the non-linear conversation efficiency, and shorten the lifetime of the crystal.[29,30] Alternatively, the laser at 447 nm can pump the OPA for generating 895 nm squeezed state of light, which is resonant with a Cs atom D_1 line for the application in light-atom quantum interfaces. Moreover, the influence of the thermal effect in a PPKTP crystal on a 447 nm laser is less than that on a 398 nm laser. Therefore, 447 nm light has been produced through direct frequency doubling of a laser at 895 nm from Cs vapor using a PPKTP crystal,[31] and then by intracavity frequency doubling of a Cs laser in a PPKTP crystal.[32] In the preparation system of a squeezed state, 50 mW blue laser is employed to pump OPA, and in particular, the generation of tripartite entangled optical fields for quantum internet needs three squeezed optical beams from OPAs, which requires a 150 mW blue laser.[11] Furthermore, the noise characteristic of pump fields of OPA influences the quality of output non-classical state of light, and the entangled degree of Einstein–Podolsky–Rosen (EPR) entangled optical fields can be improved by reducing the noise of both pump fields and signal fields of OPA to the quantum noise limit (QNL) in the squeezing frequency range of 2 MHz.[33] So far, a tunable 178 mW laser at 447 nm has been generated by frequency doubling of a tapered amplifier boosted diode laser system which reaches QNL at frequencies above 18 MHz.[34] However, the generation of higher power blue laser with low noise in MHz frequency range still remains demanding for quantum metrology and quantum network.

In this paper, we have demonstrated that a high-efficiency generation of a 447 nm laser with low noise can be experimentally realized by frequency doubling of a Ti:sapphire laser in an external ring cavity with a PPKTP crystal. Firstly, the thermal effect of a PPKTP crystal at 447 nm is reduced, compared to that at 398 nm. Secondly, the cavity configuration can influence the thermal effect. The standing-wave cavity with two mirrors is a simple configuration and has the advantage of low round trip loss. However, the blue laser in the standing-wave cavity is generated in the forward and backward direction of propagation, and the double pass absorption can result in a serious thermal effect. For a bow-tie-type ring cavity with two spherical mirrors and two flat mirrors, the optical beam travels in one direction, where no standing-wave and double-pass absorption effects happen. Thus, the bow-tie-type ring cavity is employed in our scheme to reduce the thermal effect, and makes it possible to realize a high efficiency conversion and obtain a stable high-power blue laser. The maximum output blue laser power can reach up to 308 mW with a conversion efficiency of 70%, when 440 mW fundamental wave laser is injected. The corresponding power fluctuation is 0.30% for 30 min at an input power of 300 mW. The optical beam quality factors (M^2) of output blue laser are $M_x^2 = 1.21$ and $M_y^2 = 1.26$, which is suitable for the mode matching of the input pump field to OPA. Besides, the squeezed state generated from OPA enables the reduction of noise of optical fields, and the noises of pump and signal fields are sensitive to the quality of the squeezed state. The narrow linewidth Ti:sapphire laser, which can reach QNL above the analyzing frequency of 1.5 MHz, and the frequency doubler with ring cavity configuration with 11.5 MHz linewidth, are employed together. With the help of the SHG ring cavity pumped by the Ti:sapphire laser, the noise performance of the output blue laser can be optimized, and reach QNL when the analyzing frequency is above 1.5 MHz. We, therefore, provide an ideal pump field of OPA for generating non-classical states of light resonant with a Cs atom D_1 absorption line.

The SHG of the infrared laser is one of widely used approaches to obtain the blue laser. A schematic of the experimental setup is demonstrated in Fig. 1. A continuous-wave low-noise Ti:sapphire laser (Coherent MBR110) at 895 nm pumped by Nd:YVO_4 green laser (Yuguang DPSS FG-VIIIB) is used as the injected fundamental wave laser of the SHG process. A Faraday isolator (ISO) is utilized between the Ti:sapphire laser and frequency doubling cavity to prevent the optical feedback into the Ti:sapphire laser. A half wave plate (HWP1) and the polarizing beam splitters (PBS1) are used to adjust the power of infrared laser which is incident into the SHG cavity. The bow-tie-type ring cavity configuration with the folding angle of 17 degrees, which enables the enhancement of the interaction between light and nonlinear crystal and reduces the influence of the thermal effect as a result of a single pass in the crystal, is employed in our system. The two flat mirrors and two plano-concave mirrors with a radius of curvature of 50 mm are employed to form the ring cavity. The flat mirror M1 with the transmissivity of 10% at 895 nm on one side and the antireflection at 895 nm on the other side is used as the input coupler. The flat mirror M2 has a high reflection coating at 895 nm, and the plano-concave mirrors M3 and M4 are coated with the high reflection at 895 nm and anti-reflection at 447 nm. The mirror M3 is mounted on a piezo-electric transducer (PZT) to lock the SHG cavity length resonant with the fundamental-wave laser based on the Pound–Drever–Hall (PDH) locking technique.[35,36] The infrared laser is phase modulated by an electro-optical modulator (EOM) for the locking of SHG cavity resonance. When the infrared laser is resonant in SHG cavity, a very weak infrared laser is leaked from the mirror M2, and the transmitted weak infrared laser can be detected by a 50 MHz high gain detector with a S5971 diode (PD) to generate an error signal of SHG cavity resonance locking. The mirror M4 is used as the output coupler of the blue laser. In the PDH locking technique, a high radio frequency (5.75 MHz) signal is divided into two parts, one is used to drive the EOM and the other is multiplied by the detected transmission signal of the cavity using a mixer, the output of which passes through a low pass filter and a proportional-integral-derivative (PID) controller. The generated error signal with a high signal-to-noise ratio and a large acquisition range is then used to actively lock the cavity to resonate with the pump laser. The high effective nonlinearity and walk-off free PPKTP crystal is placed in the ring cavity to realize the nonlinear interaction. The KTP crystal is periodically poled by the electric field with a poling period of 4.975 μm, so that it enables the quasi-phase-matching at an arbitrary chosen wavelength and access to the largest non-linear tensor element, which enables to make use of the maximum nonlinear coefficient. It also does not suffer from the walk-off effect. A $1 \times 2 \times 10\,\mathrm{mm}^3$ PPKTP crystal, where both sides are coated with anti-reflection at 895 nm and 447 nm, is placed in the center between two concurved mirrors. According to the theory by Ref. 37, the optical beam waist is adjusted to 23 μm, which can be calculated according to ABCD Matrix formalism when the total cavity length is 443 mm. The polarization of the incident pump laser is aligned by a half wave plate (HWP2) placed before frequency doubling cavity and the beam waist of the injected infrared laser is adjusted by means of lens system to realize the mode matching for nonlinear conversion. The fundamental wave is made matched to the enhancement cavity with the efficiency of 96.3%, which is evaluated from the contrast of the transmission fringes under cavity length scanning using PZT on M3. The crystal is wrapped by an indium foil and fixed in a copper oven, whose temperature is precisely controlled for the phase matching condition of the PPKTP crystal to realize the maximum nonlinear conversion. The SHG cavity is enclosed in a box in order to reduce the air flow and vibrations, which is necessary for a stable power output.

Two dichroic beam splitters (DBS1, DBS2) are placed after the output coupler of frequency doubling cavity and used to separate the SHG laser and a small part of the transmitted fundamental-wave laser from the output coupler. Two half wave plates HWP3, HWP4 and two polarizing beam splitters PBS2, PBS3 are used to adjust the output blue laser power for different measurements. When the output laser is reflected by PBS2, a power meter is utilized for the power measurement. While it goes through the PBS2 and reflected by PBS3, it can be measured by a beam profiler. The beam transmitted from PBS2, and PBS3 is injected into the

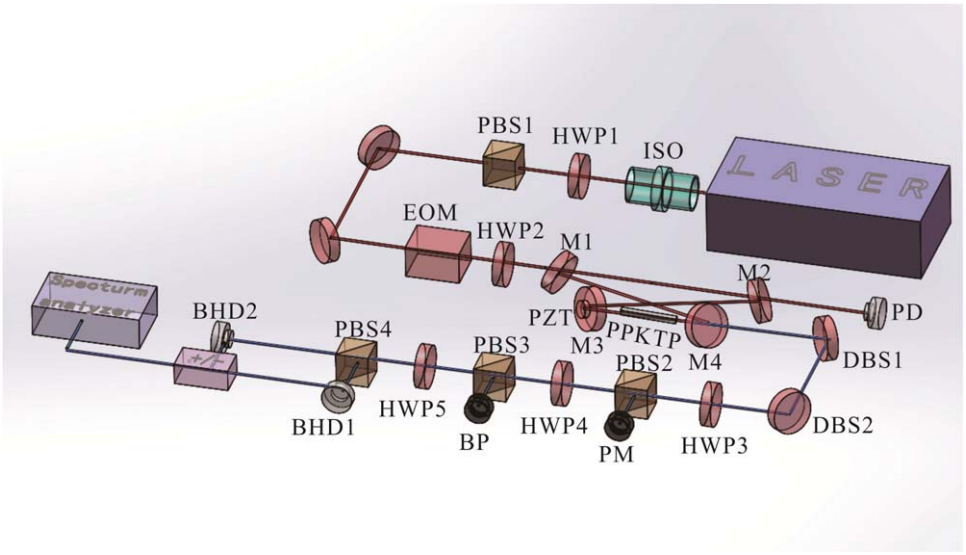

Fig. 1. (Color online) A schematic of the experimental setup. ISO: isolator; HWP1-HWP5: half-wave plate; PBS1-PBS4: polarization beam splitter; M1-M2: flat mirror; M3-M4: plano-concave mirror; DBS1-DBS2: dichroic beam splitter; PZT: piezo-electric transducer; EOM: electro-optical modulator; PM: power meter; BP: beam profiler; PD: photo detector. BHD1-BHD2: balanced homodyne detector.

self homodyne detection system, which consists of half wave plate HWP5, polarization beam splitter PBS4, and two 5 MHz balanced homodyne detectors (BHD1, BHD2) with Hamamatsu Photonics S5971 diodes, and the subtraction and sum of photon currents from these two detectors are amplified to give the quantum noise limit (QNL) and the intensity noise of blue laser, respectively.

We start by investigating the dependence of the output power $P_{2\omega}$ of the SHG laser on the input power P_{in} of incident fundamental-wave laser, which is given by[20)]

$$P_{2\omega} = \Gamma_{eff} \frac{T^2 \cdot P_{in}^2}{[1 - \sqrt{(1-T)(1-L)(1-\Gamma \cdot P_{cir})}]^4}, \quad (1)$$

where Γ is the nonlinear loss of the external cavity, as $\Gamma = \Gamma_{eff} + \Gamma_{abs}$, Γ_{eff} is the nonlinear conversion coefficient of the PPKTP crystal, and Γ_{abs} is the efficiency of the second harmonic absorption process. T is the input mirror transmissivity, and L is the intracavity loss. P_{cir} is the circulating power of the fundamental-wave laser, as $P_{cir} = T \cdot P_{in} / [1 - \sqrt{(1-T)(1-L)(1-\Gamma \cdot P_{cir})}]^2$. Therefore, the conversion efficiency η can be obtained as

$$\eta = \frac{\Gamma_{eff} \cdot T^2 \cdot P_{in}}{[1 - \sqrt{(1-T)(1-L)(1-\Gamma \cdot P_{cir})}]^4}. \quad (2)$$

The dependencies of output SHG power and its corresponding conversion efficiency on the input power of fundamental wave laser are plotted in Figs. 2 (a) and 2 (b), respectively. When the system parameters are taken into account—the input mirror transmissivity (0.1 ($T = 0.1$)), the intracavity loss (0.01 ($L = 0.01$)), the nonlinear conversion coefficient of the PPKTP crystal (0.013/W ($\Gamma_{eff} = 0.013$/W)), and the efficiency of the second harmonic absorption process (0.002 /W ($\Gamma_{abs} = 0.002$/W))—the solid lines from Eqs. (1) and (2) are the theoretical curves and the dots represent the experimental results. From Fig. 2 we can see that a maximum blue laser power of 308 mW with 440 mW incident fundamental wave power is obtained, and the corresponding conversion efficiency is 70%. If the input fundamental wave power is increased, the locking will be worse. The experimental results are lower than the theoretical curves, which is caused by the unavoidable thermal effect in the PPKTP crystal in the frequency doubling for blue laser. The heating, which induces the non-optimal phase-matching, non-optimal mode-matching, non-optimal resonant locking and bistability-like phenomenon, will decrease the maximum output power of the blue laser and cause the conversion efficiency to get worse. Due to a single pass in the PPKTP in the ring cavity, the influence of thermal effect in the ring cavity is smaller than that in the standing-wave cavity. Thus the better output power and conversion efficiency can be obtained, compared to the case in the standing-wave cavity.[34)] The inserts are the cavity resonant signal of infrared and blue lasers with the optimal phase-matching temperature at the input power of 440 mW. It can be seen that for the 447 nm laser, the thermal effect of PPKTP crystal in ring cavity and its induced bi-stability-like phenomenon are not very severe.

The output power stabilities of the Ti:sapphire laser and blue laser over 30 min are measured by a power meter (Thorlabs S305C), as shown in Fig. 3. The blue laser power stability is limited by the power stability of incident fundamental wave laser, the thermal effect and locking system. In our system, the root mean square (RMS) of the Ti:sapphire laser is 0.06% at the injection fundamental wave power of 300 mW and the RMS of blue laser is 0.07% at the injection fundamental wave power of 200 mW. The RMS of blue laser can be kept to 0.30% when the input infrared laser is increased to 300 mW. In our system, the M^2 values for x and y axes are $M_x^2 = 1.21$ and $M_y^2 = 1.26$, respectively, when the injection fundamental wave power is 300 mW, and is beneficial for good model matching. The frequency of the SHG cavity can be tuned as a result of good frequency tunability of the Ti:sapphire laser. Together with the Ti:sapphire laser, the tunable blue laser enables the preparation of the non-classical light matching of the Cs atom D1 absorption line.

The normalized intensity noise spectra for the fundamental wave laser and second harmonic laser with different input

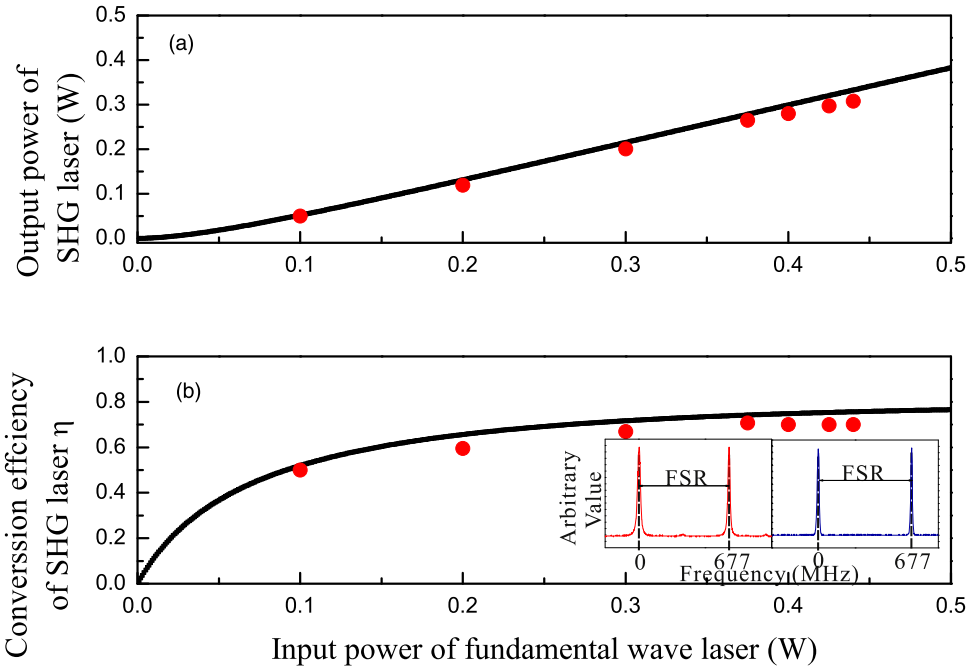

Fig. 2. (Color online) The dependencies of output SHG power (a) and its corresponding conversion efficiency (b) on the input power of the fundamental wave laser. The solid lines and dots are for theoretical and experimental results, respectively. The inserts are the infrared (left) and blue (right) lasers versus cavity length change with the optimal phase-matching temperature at the input power of 440 mW.

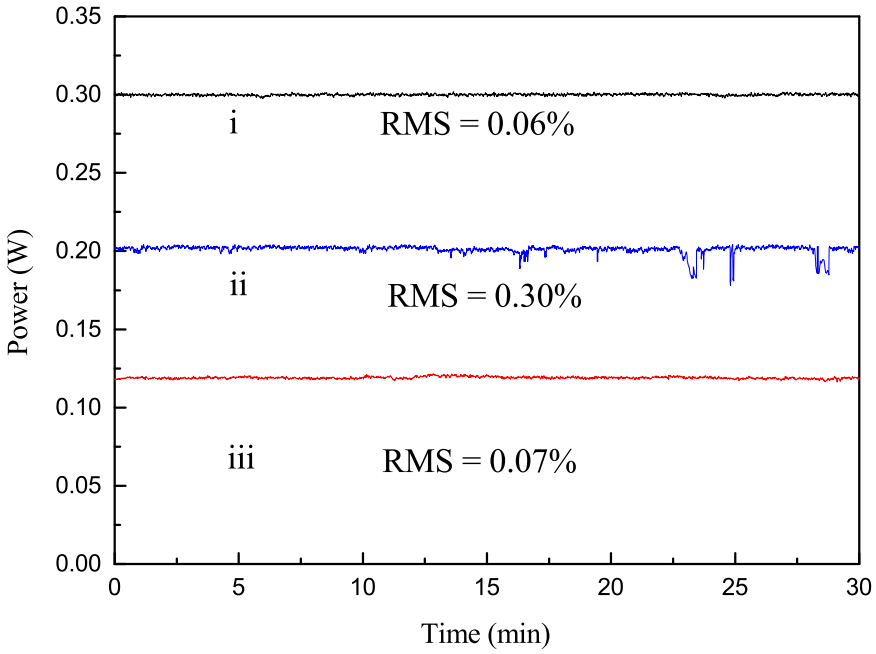

Fig. 3. (Color online) The output power stability of the laser about 30 min. Trace i is the power stability of infrared laser at the input power $P_{in} = 300$ mW; and trace ii and iii are the power stability of blue laser at the input powers $P_{in} = 300$ mW and $P_{in} = 200$ mW, respectively.

power for $P_{in} = 100$ mW, 200 mW, 300 mW are demonstrated in Figs. 4(a)–4(d), respectively. The characteristics of the intensity noise of the blue laser is measured by the self-homodyne detection system. The trace i is the QNL, which is obtained from the subtraction of amplified photon currents, and trace ii is the intensity noise from the sum of amplified photon currents. The noise spectrum is recorded and analyzed by a spectrum analyzer with the resolution bandwidth of 30 KHz and the video bandwidth of 100 Hz. From Fig. 4, we can see that the noise of the narrow linewidth Ti:sapphire laser can reach QNL with the input power of 300 mW when the analyzing frequency above 1.5 MHz. By employing the bow-tie ring frequency doubling, the intensity noises reach the QNL for different incident fundamental wave laser power of 100 mW, 200 mW, 300 mW, respectively, when the analyzing frequency is above 1.5 MHz. Usually, the quantum noise of the squeezed state is analyzed at $2 \sim 3$ MHz, and thus we provide suitable high-power laser with low noise for the pump field of OPA.[9,11] Therefore, our system can provide blue laser with high conversation efficiency, stable high power and low noise. Which meet the requirement of the pump field of OPA for generating squeezed light or

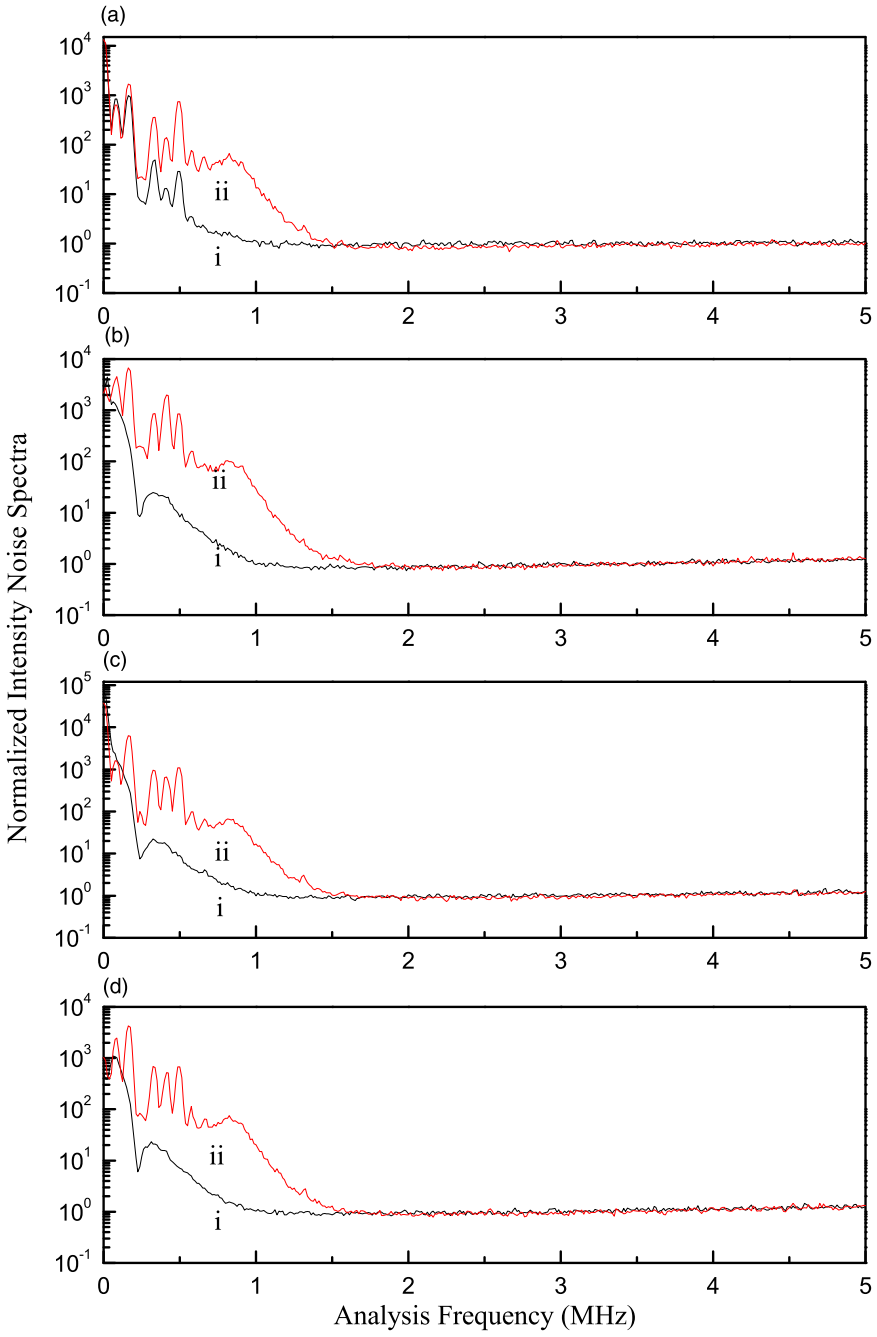

Fig. 4. (Color online) The normalized noise spectra for fundamental field with input power $P_{in} = 300$ mW (a), and SHG fields with different input power: $P_{in} = 100$ mW (b), $P_{in} = 200$ mW (c), $P_{in} = 300$ mW (d). Trace i is the QNL and trace ii is the intensity noise.

entangled optical modes resonant with the Cs atom D_1 absorption line.

In summary, we demonstrate a high-efficiency generation of the low-noise 447 nm laser by frequency doubling of the Ti:sapphire laser in an external ring cavity with PPKTP crystal. Compared to previous work,[34] the thermal effect can be reduced by employing a bow-tie-type ring cavity instead of a standing-wave cavity, and the high-efficiency conversion with stable out power can be obtained. We obtain the maximum SHG power of 308 mW and the corresponding conversion efficiency of 70%, when the power of incident fundamental wave is 440 mW. At the input infrared laser power of 300 mW, the power stability is less than 0.30% for 30 min, and the beam quality factors are $M_x^2 = 1.21$ and $M_y^2 = 1.26$, respectively. Furthermore, the noises of pump and signal fields of OPA are very important for the OPA based generation system of squeezed state. By employing low noise Ti:sapphire laser and bow-tie-type ring configuration, the noise of blue laser can reach the QNL when the frequency is above 1.5 MHz. The resulting high-power, low-noise blue laser is suitable for generating non-classical state of light, such as multipartite entangled optical fields resonant with Cs atom D_1 line, and can be applied in quantum information science.

Acknowledgments The Key Project of the Ministry of Science and Technology of China (Grant No. 2016YFA0301402), the Natural Science Foundation of China (Grants Nos. 61775127, 11474190, 11654002, 11834010), the Program for Sanjin Scholars of Shanxi Province, Program for the Outstanding Innovative Teams of Higher Learning Institutions of Shanxi, Shanxi Scholarship Council of China, and the fund for Shanxi "1331 Project" Key Subjects Construction.

1) M. R. Huo, J. L. Qin, J. L. Cheng, Z. H. Yan, Z. Z. Qin, X. L. Su, X. J. Jia, C. D. Xie, and K. C. Peng, Sci. Adv. **4**, 9401 (2018).
2) Y. Y. Zhou, J. Yu, Z. H. Yan, X. J. Jia, J. Zhang, C. D. Xie, and K. C. Peng, Phys. Rev. Lett. **121**, 150502 (2018).
3) H. Sasakura, S. Muto, and H. Kumano, Appl. Phys. Express **8**, 112002 (2015).
4) F. Wolfgramm, A. Cere, F. A. Beduini, A. Predojevic, M. Koschorreck, and M. W. Mitchell, Phys. Rev. Lett. **105**, 053601 (2010).
5) H. J. Kimble, Nature **453**, 1023 (2008).
6) J. I. Cirac, P. Zoller, H. J. Kimble, and H. Mabuchi, Phys. Rev. Lett. **78**, 3221 (1997).
7) Y. H. Liu, J. L. Yan, L. X. Ma, Z. H. Yan, and X. J. Jia, Phys. Rev. A **98**, 052308 (2018).
8) Z. H. Yan and X. J. Jia, Quantum Science and Technology **2**, 024003 (2017).
9) Z. H. Yan, L. Wu, X. J. Jia, Y. H. Liu, R. J. Deng, S. J. Li, H. Wang, C. D. Xie, and K. C. Peng, Nature Commun. **8**, 718 (2017).
10) Z. H. Yan, Y. H. Liu, J. L. Yan, and X. J. Jia, Phys. Rev. A **97**, 013856 (2018).
11) L. Wu, Z. H. Yan, Y. H. Liu, R. J. Deng, X. J. Jia, C. D. Xie, and K. C. Peng, Appl. Phys. Lett. **108**, 161102 (2016).
12) H. Vahlbruch, M. Mehmet, K. Danzmann, and R. Schnabel, Phys. Rev. Lett. **117**, 110801 (2016).
13) N. Ishii, K. Kitano, T. Kanai, S. Watanabe, and J. Itatani, Appl. Phys. Express **4**, 022701 (2011).
14) P. Grangier, R. E. Slusher, B. Yurke, and A. LaPorta, Phys. Rev. Lett. **59**, 2153 (1987).
15) E. S. Polzik, J. Carri, and H. J. Kimble, Phys. Rev. Lett. **68**, 3020 (1992).
16) K. H. Honda, D. S. Akamatsu, M. B. Arikawa, Y. H. Yokoi, K. C. Akiba, S. S. Nagatsuka, T. H. Tanimura, A. Furusawa, and M. Kozuma, Phys. Rev. Lett. **100**, 093601 (2008).
17) J. G. Appel, E. Figueroa, D. Korystov, M. Lobino, and A. I. Lvovsky, Phys. Rev. Lett. **100**, 093602 (2008).
18) J. E. Hastiea, L. G. Morton, A. J. Kemp, and M. D. Dawson, Appl. Phys. Lett. **89**, 061114 (2006).
19) J. H. Lundeman, O. B. Jensen, P. E. Andersen, S. Andersson-Engels, B. Sumpf, G. Erbert, and P. M. Petersen, Opt. Express **16**, 2486 (2008).
20) R. L. Targat, J. J. Zondy, and P. Lemonde, Opt. Commun. **247**, 471 (2005).
21) I. Juwiler, A. Arie, A. Skliar, and G. Rosenman, Opt. Lett. **24**, 1236 (1999).
22) F. Villa, A. Chiummo, E. Giacobino, and A. Bramati, J. Opt. Soc. Am. B **24**, 576 (2007).
23) T. Tanimura, D. Akamatsu, Y. Yokoi, A. Furusawa, and M. Kozuma, Opt. Lett. **31**, 2344 (2006).
24) G. Hetet, O. Glockl, K. A. Pilypas, C. C. Harb, B. C. Buchler, H. A. Bachor, and P. K. Lam, J. Phys. B, At. Mol. Opt. Phys. **40**, 221 (2007).
25) A. Predojevic, Z. Zhai, J. M. Caballero, and M. W. Mitchell, Phys. Rev. A **78**, 063820 (2008).
26) S. Burks, J. Ortalo, A. Chiummo, X. J. Jia, F. Villa, A. Bramati, J. Laurat, and E. Giacobino, Opt. Express **17**, 3777 (2009).
27) J. Jing, C. Kiu, Z. Zhou, Z. Ou, and W. Zhang, Appl. Phys. Lett. **99**, 011110 (2011).
28) M. Pizzocaro, D. Calonico, P. C. Pastor, J. Catani, G. A. Costanzo, F. Levi, and L. Lorini, Appl. Opt. **53**, 3388 (2014).
29) M. Sabaeian, L. Mousave, and H. Nadgaran, Opt. Express **18**, 18732 (2010).
30) W. H. Yang, Y. J. Wang, Y. H. Zheng, and H. D. Lu, Opt. Express **23**, 19624 (2015).
31) B. V. Zhdanov, Y. L. Lu, M. K. Shaffer, W. Miller, D. Wright, and R. J. Knize, Opt. Express **16**, 17585 (2008).
32) B. V. Zhdanov, M. K. Shaffer, W. Holmes, and R. J. Knize, Opt. Commun. **282**, 4585 (2009).
33) Y. Wang, H. Shen, X. L. Jin, X. L. Su, C. D. Xie, and K. C. Peng, Opt. Express **18**, 6149 (2010).
34) Y. Zhang, J. H. Liu, J. Z. Wu, R. Ma, D. Wang, and J. X. Zhang, Opt. Express **24**, 19769 (2016).
35) R. V. Pound, Review of Scientific Instrum. **17**, 490 (1946).
36) R. W. P. Drever, J. L. Hall, F. V. Kowalski, J. Hough, G. M. Ford, A. J. Munley, and H. Ward, Appl. Phys. B **31**, 97 (1983).
37) G. D. Boyd and D. A. Kleinman, J. Appl. Phys. **39**, 3597 (1986).
38) M. R. Huo, J. L. Qin, Y. R. Sun, J. L. Cheng, Z. H. Yan, and X. J. Jia, Acta Sin. Quantum Opt. **24**, 134 (2018).